Synthesis and properties of liquid pyrazine dyes

Jae-Young Lee[a], Tetsuya Aoyama[b], Masanobu Uchiyama[b,c], Shinya Matsumoto[a,*]

[a]Graduate School of Environment and Information Sciences, Yokohama National University, 79-7 Tokiwadai, Yokohama 240-8501, Japan

[b]RIKEN Cluster for Pioneering Research (CPR), 2-1 Hirosawa, Wako, Saitama 351-0198, Japan

[c]Graduate School of Pharmaceutical Sciences, The University of Tokyo, 7-3-1 Hongo, Bunkyo-ku, Tokyo 113-0033, Japan

*Corresponding author.

E-mail address: matsumoto-shinya-py@ynu.ac.jp

Abstract

Six 2,5-diamino-3,6-dicyanopyrazine dyes with medium to long length alkyl chains on their amino groups were newly synthesised and their fundamental properties investigated, including their derivatives, focusing on liquefaction at room temperature. The butyl, pentyl, hexyl, heptyl, octyl, and dodecyl substitutions realised liquefaction of the dye chromophore. These liquid dyes exhibited relatively good fluorescent properties in the liquid state. The dodecyl derivative showed the largest fluorescence efficiency of 0.59 in the liquid state among the derivatives and was used in an organic light-emitting device. The efficient yellow EL emission peaked at 593 nm with a 10 V turn-on voltage of the device and a maximum brightness of 336 cd/m^2 at 14 V.

Keywords: Pyrazine dye, Fluorescent dye, Liquid dye, Optical property, Organic light-emitting diode.

1. Introduction

Liquid dyes are organic dyes that are liquids at room temperature. Recently, their unique physicochemical properties have attracted significant interest for their potential in optoelectronic applications, and particularly in flexible optoelectronic devices because of their flexibility and adaptability to printable processes [1–7]. It is also a great advantage that many technologies for manufacturing liquid crystal displays can use liquid dyes.

The syntheses of liquid dyes have been reported for several dye systems including coumarins [8], perfluorophenazines [9], fullerenes [10], and azo compounds [11] with various substituents such as linear or branched dialkylamino, alkoxy, and alkyl groups. In previous reports, the melting points of functionalised organic dyes have been shown to decrease with long flexible chain substituents, sometimes becoming viscous oils or fluids at room temperature. This highlighted the effects of substituents on the melting point, although the number of related studies is limited compared with that of liquid crystalline organic compounds [12,13]. Thus, it remains difficult to identify the precise mechanism of liquefaction. In this study, liquid dyes were prepared based on the 2,5-diamino-3,6-dicyanopyrazine chromophore (**1**), as shown in Fig. 1.

Pyrazine rings have been widely used as electron acceptors for constructing electron-deficient parts of molecules [14]. Furthermore, pyrazine derivatives are easily functionalised by substitution of donor groups at the 2, 3, 5, 6-positions, resulting in a small CT state with a separation of the HOMO and the LUMO [15]. Some pyrazine dyes have been reported to exhibit several different solid forms with different

optical properties [16–18]. 2,5-Diamino-3,6-dicyanopyrazine (**1**) shown in Fig. 1 exhibits an intense yellowish-green fluorescence in solution, while it is non-emissive in the solid state [19]. When the amino groups of the compound are modified with bulky halogen- or methyl-substituted benzyl groups, the obtained derivatives exhibit intense orange fluorescence both in solution and the solid state [20]. Previous studies of the pyrazine dyes with Cl/Br-substituted benzyl groups exhibited polymorphism [21,22], with their crystal structures suggesting that the colour change was caused by conformational differences in the solid state. [18,23–25]

In this study, a systematic examination of the optical properties of liquid pyrazine dyes based on the 2,5-diamino-3,6-dicyanopyrazine chromophore was performed by altering the chain length of the alkyl substituents on the amino groups, as shown in Fig. 1. The synthesis and basic optical properties of several liquid derivatives were reported while focusing on the effects of the pyrazine dye alkyl groups on the melting point and photophysical properties. The liquid dye with the largest fluorescence efficiency among the prepared liquid dyes was also examined for its potential as an emitter material in organic light emitting diodes (OLEDs).

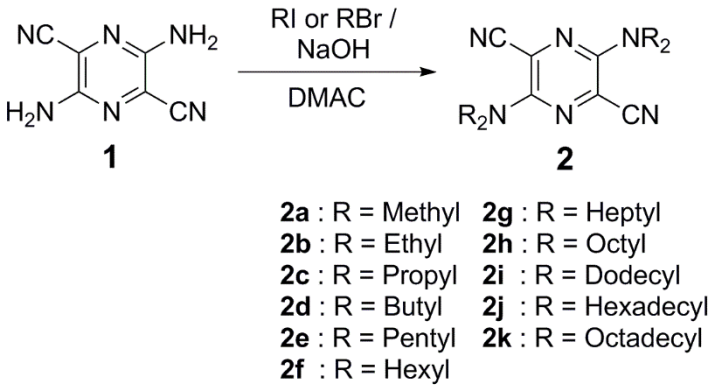

Figure 1. Chemical structures of pyrazine dyes **2a**–**2k**.

2. Experimental

2.1. Materials

The alkyl iodides (97%) were purchased from Tokyo Chemical Industry Co. (TCI). Sodium hydroxide (97%) was obtained from Wako Pure Chem. Ind., Ltd. Wako silica gel C-300 (45–75 mm) was used for column chromatography and 2,5-diamino-3,6-dicyanopyrazine was supplied from Nippon Soda Co. Ltd. **2d**–**2k** were synthesised following a previously reported procedure [19,20]. Structural characterisation was performed using nuclear magnetic resonance (NMR) spectroscopy, Fourier transform infrared (FT-IR) spectroscopy, and high-resolution mass spectrometry (HRMS). The NMR spectra were

recorded in $CDCl_3$, unless otherwise stated, with tetramethylsilane (TMS) as an internal reference at ambient temperature, using a DRX 300 MHz spectrometer (Bruker Co.) and JNM-ECX 400 MHz spectrometer (Jeol Resonance Co.). The FT-IR spectra were collected using a Jasco FT/IR-6200 spectrometer. The HRMS data and liquid chromatography-electrospray ionisation mass spectrometry (LC-ESI-MS) spectra were recorded using a LaChrom ultra-high performance liquid chromatography system coupled to a time-of-flight (ToF) mass spectrometer (Nano Frontier LD, Hitachi High-Technologies Co.). The melting points (T_m) of the prepared compounds were measured by differential scanning calorimetry (DSC) using a Rigaku ThermoPlus DSC 8230 instrument at a heating rate of 10 °C/min and an air flow rate of 10 mL/min. Cyclic voltammetry was performed using an electrochemical analyser Model 760Dz (ALS/H CH Instruments) at room temperature in nitrogen purged CH_2Cl_2 with a tetrabutylammoniumhexafluorophosphate ($TBAPF_6$) supporting electrolyte at a scanning rate of 100 mV/s. A glassy carbon, Pt wire, and $Ag/AgNO_3$ were used as the working, counter, and reference electrodes, respectively. The oxidation potential was calibrated with ferrocene and the energy gap between the highest occupied molecular orbital (HOMO) and lowest unoccupied molecular orbital (LUMO) was estimated using the UV-vis absorption spectrum edge.

2.2. General procedure for synthesis of 2,5-bis(*N*,*N*-dialkylamino)-3,6-dicyanopyrazines (2)

To a 50 mL flask cooled with ice, 2,5-diamino-3,6-dicyanopyrazine **1** (3 mmol) and alkyl iodide (**2d–2k**; 30 mmol) were dissolved in dimethylacetamide (30 mL) and sodium hydroxide (15 mmol) was slowly added with stirring. The ensuing mixture was then stirred at room temperature for 1–3 h. After completion of the reaction, distilled water (60 mL) was added to the reaction mixture and the liquor was extracted using ethyl acetate. The extract was evaporated to afford a residue which was purified by column chromatography on silica gel with EtOAc/*n*-hexane (1/3, v/v) as an eluent. Compounds **2a–2e** were previously reported [19,20].

2.2.1. 2,5-bis(*N*,*N*-dihexylamino)-3,6-dicyanopyrazines (2f)

Yield 3.4%. ^{1}H NMR (300 MHz, $CDCl_3$) δ: 0.89 (t, 12H, J = 6.78 Hz), 1.26–1.35 (m, 24H), 1.57–1.62 (m, 8H), 3.46 (t, 8H, J = 7.91 Hz) ppm; ^{13}C NMR (75 MHz, $CDCl_3$) δ: 14.01, 22.6, 26.4, 27.84, 31.56, 50.32, 112.74, 116.68, 148.87 ppm; IR (neat, cm^{-1}) 2928, 2216, 1509, 1465, 1214; ESI MS: *m/z* 497.43 $[M+H]^+$; HRMS (ESI) *m/z* calcd. for $C_{30}H_{53}N_6$ $[(M+H)^+]$ 497.43262, found 497.43153.

2.2.2. 2,5-bis(*N*,*N*-diheptylamino)-3,6-dicyanopyrazines (2g)

Yield 4.4%. ^{1}H NMR (400 MHz, $CDCl_3$) δ: 0.87 (t, 12H, J = 6.4 Hz), 1.26–1.31 (m, 32H), 1.57–1.63 (m, 8H), 3.45 (t, 8H, J = 7.8 Hz) ppm; ^{13}C NMR (100 MHz, $CDCl_3$) δ: 14.16, 22.68, 26.79, 27.79, 29.14, 31.86, 50.40, 112.82, 116.78, 148.95 ppm; IR (neat, cm^{-1}) 2924, 2215, 1508, 1464, 1217; ESI MS: *m/z* 553.49 $[M+H]^+$; HRMS (ESI) *m/z* calcd. for $C_{34}H_{61}N_6$ $[(M+H)^+]$ 553.49522, found 553.49400.

2.2.3. 2,5-bis(*N,N*-dioctylamino)-3,6-dicyanopyrazines (2h)

Yield 3.3%. ^{1}H NMR (400 MHz, $CDCl_3$) δ: 0.87 (t, 12H, J = 7.33 Hz), 1.26–1.29 (m, 40H), 1.57–1.65 (m, 8H), 3.45 (t, 8H, J = 8.7 Hz) ppm; ^{13}C NMR (100 MHz, $CDCl_3$) δ: 14.18, 22.73, 26.83, 27.97, 29.32, 29.44, 31.88, 50.40, 112.83, 116.78, 148.95 ppm; IR (neat, cm^{-1}) 2924, 2216, 1506, 1464, 1215; ESI MS: *m/z* 609.55 $[M+H]^+$; HRMS (ESI) *m/z* calcd. for $C_{38}H_{69}N_6$ $[(M+H)^+]$ 609.55782, found 609.55570.

2.2.4. 2,5-bis(*N,N*-didodecylamino)-3,6-dicyanopyrazines (2i)

Yield 4.2%. ^{1}H NMR (300 MHz, $CDCl_3$) δ: 0.82 (t, 12H, J = 6.4 Hz), 1.21–1.35 (m, 72H), 1.75 (quint, 8H, J = 7.16 Hz), 3.09 (t, 8H, J = 6.97 Hz) ppm; ^{13}C NMR (100 MHz, $CDCl_3$) δ: 7.38, 14.22, 22.78, 28.65, 29.44, 29.53, 29.65, 29.72, 30.61, 32.01, 33.68, 50.40, 112.83, 116.76, 148.95 ppm; IR (neat, cm^{-1}) 2925, 2212, 1509, 1465, 1216; ESI MS: *m/z* 833.80 $[M+H]^+$; HRMS (ESI) *m/z* calcd. for $C_{54}H_{101}N_6$ $[(M+H)^+]$ 833.80822, found 833.80630.

2.2.5. 2,5-bis(*N,N*-dihexadecylamino)-3,6-dicyanopyrazines (2j)

Yield 1.5%. ^{1}H NMR (400 MHz, $CDCl_3$) δ: 0.87 (t, 12H, J = 6.4 Hz), 1.25–1.29 (m, 104H), 1.57–1.64 (m, 8H), 3.44 (t, 8H, J = 7.33 Hz) ppm; ^{13}C NMR (100 MHz, $CDCl_3$) δ: 14.21, 22.78, 26.85, 27.99, 29.46, 29.51, 29.70, 29.76, 29.79, 32.02, 50.40, 112.82, 116.78, 148.96 ppm; IR (KBr, cm^{-1}) 2918, 2218, 1512, 1469, 1219; ESI MS: *m/z* 1058.05 $[M+H]^+$; HRMS (ESI) *m/z* calcd. for $C_{70}H_{133}N_6$ $[(M+H)^+]$ 1058.05863, found 1058.05395.

2.2.6. 2,5-bis(*N,N*-dioctadecylamino)-3,6-dicyanopyrazines (2k)

Yield 1.7%. ^{1}H NMR (400 MHz, $CDCl_3$) δ: 0.87 (t, 12H, J = 6.87 Hz), 1.24–1.29 (m, 120H), 1.58–1.64 (m, 8H), 3.44 (t, 8H, J = 7.79 Hz) ppm; ^{13}C NMR (100 MHz, $CDCl_3$) δ: 14.21, 22.78, 26.85, 27.99, 29.46, 29.51, 29.70, 29.80, 32.01, 50.40, 112.82, 116.78, 148.96 ppm; IR (KBr, cm^{-1}) 2919, 2218, 1512, 1470, 1221; ESI MS: *m/z* 1170.14 $[M+H]^+$; HRMS (ESI) *m/z* calcd. for $C_{78}H_{149}N_6$ $[(M+H)^+]$ 1170.18383, found 1170.17817.

2.3. Characterisation of photophysical properties and molecular orbital calculations

The UV-vis absorption spectra of **2d–2k** in chloroform solution and neat liquids were recorded using a Perkin-Elmer Lambda 750 spectrometer, and those of the solids were recorded using an optical waveguide SIS-50 surface/interface spectrometer (SIS Co.). The fluorescence spectra of chloroform solutions and neat forms were recorded using a Jasco FP-8500 spectrofluorometer. For the spectral measurements, the liquid dyes were sandwiched by two glass plates. The excitation wavelength for the solution sample was 521 nm for **2d**–**2k** and was determined by the absorption maximum in chloroform solution. The excitation wavelength for the liquid and solid samples was 517 nm, as determined by their absorption maximum in neat form. The absolute fluorescence quantum yields (ϕ_f) of the derivatives in chloroform solution and neat forms were estimated using the spectrofluorometer with an integrating sphere system. The UV-vis absorption spectra, fluorescence spectra, and fluorescence quantum yields were measured in triplicate at room temperature. Molecular geometry optimisation and calculations of the theoretical absorption properties were performed using the Gaussian 16 program package.[26] The optimisation was performed using density functional theory, Becke's three-parameter hybrid exchange functional, and Lee-Yang-Parr non-local correlation functional (B3LYP) [27], 6-31G+(d,p) basis set. Based on the optimised molecular structure, the theoretical absorption properties were obtained by calculating the excited states using the same basis set.

2.4. OLED fabrication and measurement

Indium tin oxide (ITO) substrates were sequentially ultrasonicated in each of pure water, 2-propanol, acetone, and chloroform for 10 min. The samples were then maintained under ozone atmosphere for 3 min using a UV-ozone cleaner (PL16-110D, SEN Lights Corp., Japan). Poly(3,4-ethylenedioxythiophene) (PEDOT):poly(styrenesulfonate) (PSS) films were spin-coated onto the ITO substrates and dried at 100 °C for 1 h. An emission layer (35 nm) of poly(9,9-dioctylfluorene-alt-benzothiadiazole) (F8BT) doped with liquid fluorescent dye **2i** (40 wt%) was prepared via spin-coating from a chloroform solution at 3000 rpm onto the PEDOT:PSS-coated ITO substrates. After drying the emission layer, an electron transport layer (35 nm) composed of 1,3,5-tri(m-pyridin-3-ylphenyl)benzene (TmPyPB) was prepared via vacuum deposition. Subsequently, a cathode consisting of LiF (0.4 nm) and Al (80 nm) was thermally evaporated to form the OLEDs. The luminance-voltage characteristics were obtained using a luminance meter (LS-100, Konica Minolta) and source meter unit (model 2400, Keithley). The electroluminescence (EL) spectra were measured using a spectrometer (FLAME-S-VIS-NIR-ES, Ocean Optics).

For photoluminescence measurements, the neat and **2i**-doped F8BT films were spin-coated from a chloroform solution at 3000 rpm on top of precleaned fused silica substrates. For the neat liquid dye **2i**, the

compound was sandwiched between two fused silica substrates. The photoluminescence (PL) spectra were measured using a spectrofluorophotometer (RF-5301PC, Shimadzu).

3. Results and discussion

As shown in Fig. 1, the pyrazine dyes **2** were synthesised via substitution reactions of alkyl halides. The syntheses and optical properties of **2a**–**2e** in solution and solid films have already been reported.[19,20] The structure and purity of dyes **2f**–**2k** was confirmed via ^{1}H and ^{13}C-NMR, FT-IR, and HRMS studies. Among the reported dyes **2a**–**2e**, **2d** and **2e** were liquids at room temperature. In addition to these two dyes, the pyrazine dyes **2** containing hexyl, heptyl, octyl, and dodecyl chains were liquids at room temperature, whereas the dyes with hexadecyl and octadecyl chains were solids.

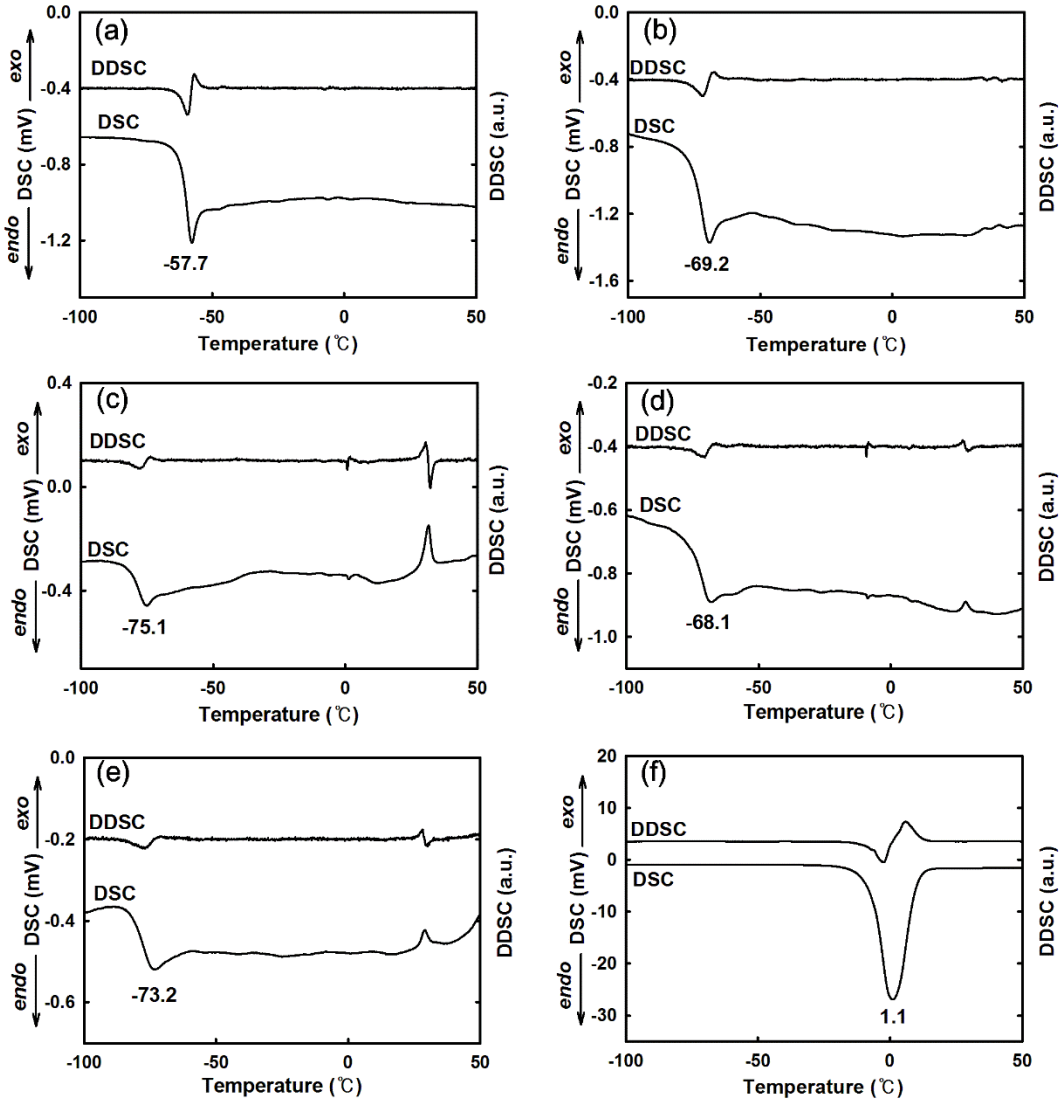

Figure 2. DSC and differential curves (DDSCs) of liquid dyes heated from -100 to 50 °C at 10 °C min^{-1}: (a) **2d**, (b) **2e**, (c) **2f**, (d) **2g**, (e) **2h**, and (f) **2i**.

3.1. Melting point

The liquid pyrazine dyes **2d**–**2i** were viscous liquids at room temperature. Even when stored at room temperature for several months, no crystals and/or powders formed and Fig. 2 shows the DSC results of the liquid derivatives. Dye **2d** exhibited an endothermic peak with a ΔH of 1.54 J/g at -57.7 °C, corresponding to the change from solid to liquid phase and no peak was observed up to 50 °C. Dyes **2e**– **2i** showed similar thermal behaviour to that of **2d**. The melting points of **2e**–**2h** were observed at -69.2, -75.1, -68.1, and -73.2 °C, respectively. Only **2i** exhibited a large endothermic peak at 1.1 °C, as shown in Fig. 2(f). The heat of fusion was calculated to be 94.7 J/g, which is significantly larger than those of the other

liquid derivatives. Zhang *et al.* reported that larger fusion enthalpies (ΔH) tend to increase the melting temperature, whereas lager fusion entropies (ΔS) tend to decrease the melting temperature [28]. These two factors compete with each other and the balance between ΔH and ΔS determines the melting point. Their results for the long alkyl chain ionic liquids showed that the increase in ΔH is more significant than that in ΔS when the alkyl chain length increases. Therefore, the results presented herein suggest that the dye **2i** exhibited high heat capacity and high melting point due to its long dodecyl groups.

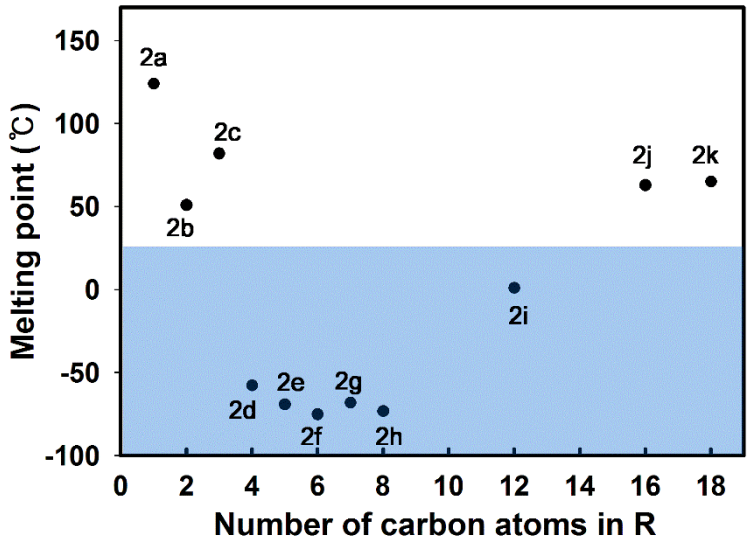

Figure 3. The relationship between melting point and the number of carbon atoms of the alkyl substituents.

The melting point data were plotted as a function of the number of carbon atoms in the alkyl chain of the pyrazine dyes (Fig. 3). From the methyl (**2a**) to butyl (**2d**) derivatives, the melting points drastically decreased with increasing number of carbon atoms in the alkyl substituent. From the butyl (**2d**) to octyl (**2h**) derivatives, the change in melting points slightly decreased with increasing number of carbon atoms in the alkyl substituent. The melting point of derivatives with longer alky chains than **2h** increased. The observed trends between the alkyl chain length and melting point were similar to the results reported in previous studies of liquid dyes [1–4,29].

The liquid state of an organic dye at room temperature is considered to be controlled by the balance between π-π interaction with respect to the chromophoric part and van der Waals interactions among the incorporated alkyl chains [3], even though this issue remains a matter of discussion. When the alkyl chain lengths are short, the π-π interaction between dye molecules is dominant and the melting points increase. In contrast, when the alkyl chain lengths are very long, the contribution of van der Waals interactions

between adjacent alkyl chains increases, resulting in a gradual increase in the melting point with the elongating alkyl chain length. When the alkyl groups are of medium size, it is reasonable to suggest that the π-π interactions are balanced with van der Waals interactions to realise a liquid dye at room temperature [30].

Table 1. Melting point and optical properties of the prepared pyrazine dyes **2a**–**2k**.

Compound	R	Mp (°C)	In chloroform					Crystalline or neat form				$\Delta\lambda$ (nm)[f]	ΔF (nm)[g]
			λ_{max} (nm)	log ε	F_{max} (nm)[a]	Φ_f[b]	SS (cm^{-1})[c]	λ_{max} (nm)	F_{max} (nm)[d]	Φ_f[b]	SS (cm^{-1})[e]		
2a	CH_3	124.5[h]	498[h]	3.64[h]	601[h]	0.55[h]	-3441	592[h]	623[h]	0.26[h]	-841	61	32
2b	C_2H_5	51[h]	516[h]	3.42[h]	602[h]	0.70[h]	-2769	553[h]	608[h]	0.14[h]	-1636	32	40
2c	C_3H_7	82[h]	520[h]	3.82[h]	607[h]	0.56[h]	-2756	586[h]	625[h]	0.26[h]	-1065	71	49
2d	C_4H_9	-57.7[i]	521	3.58	606	0.53	-2692	517	598	0.10	-2620	-4	-8
2e	C_5H_{11}	-69.2[i]	521	3.51	606	0.48	-2692	519	603	0.04	-2684	-2	-3
2f	C_6H_{13}	-75.1[i]	521	3.17	602	0.47	-2583	515	604	0.04	-2861	-6	2
2g	C_7H_{15}	-68.1[i]	523	3.63	604	0.50	-2564	518	594	0.33	-2470	-5	-10
2h	C_8H_{17}	-73.2[i]	523	3.64	604	0.49	-2564	515	598	0.27	-2695	-8	-6
2i	$C_{12}H_{25}$	1.1[i]	523	3.53	602	0.45	-2509	513	582	0.59	-2311	-10	-20
2j	$C_{16}H_{33}$	63[i]	523	3.55	603	0.53	-2537	516	601	0.50	-2741	-7	-2
2k	$C_{18}H_{37}$	65.1[i]	523	3.56	601	0.50	-2482	525	601	0.47	-2409	2	0

[a]F_{max} (solution) excited at 521 nm for **2d**–**2k**. [b]Φ: Fluorescence quantum yield. [c]SS: Stokes shift, F_{max} - λ_{max} in chloroform solution. [d]F_{max} (neat) excited at 517 nm for **2d**–**2k**. [e]SS: Stokes shift, F_{max} - λ_{max} in neat form. [f]$\Delta\lambda = \lambda_{max}$ (neat) - λ_{max} (solution). [g]$\Delta F = F_{max}$ (neat) - F_{max} (solution). [h]Reference. [i]Measured by DSC.

3.2. UV-Vis absorption and fluorescence spectra

The absorption and fluorescence properties of the prepared pyrazine dyes **2a**–**2k** in chloroform and liquid or powder state were determined to examine the substituent effects on their electronic states. The results are summarised in Table 1, where the differences in λ_{max} and F_{max} from the neat to solution state are indicated by $\Delta\lambda$ and ΔF, respectively, and the Stokes shift is denoted by SS. In a previous study [20], dye **2a** exhibited λ_{max} at 498 nm in chloroform but at 592 nm in the solid state. A large bathochromic shift of 94 nm was observed, which may be caused by the strong intermolecular π–π interactions of the pyrazine chromophore in the solid state. However, the fluorescence quantum yield of dye **2a** in the crystalline state was lower than that when dissolved in chloroform solution.

No significant influence of the alkyl chain length on the optical properties of the present pyrazine dyes in chloroform was observed. The absorption and fluorescence spectra of dyes **2d**–**2k** in chloroform solution are shown in Fig. 4(a) and (b), respectively. The first absorption maximum indicated a slight bathochromic shift with longer alkyl groups from butyl (**2d**, 521 nm) to octadecyl (**2k**, 523 nm). The fluorescence maximum indicated a sharp band at approximately 600 nm. In addition, despite changing the alkyl substituents on the nitrogen atoms of dyes **2d**–**2k,** no significant differences were observed in the spectral shape of the absorption and fluorescence spectra. This indicates that dyes **2d**–**2k** in chloroform solution possess similar electronic states and exhibited medium to high fluorescence quantum yield (ϕ_f) in the range from 0.45 to 0.70 in chloroform.

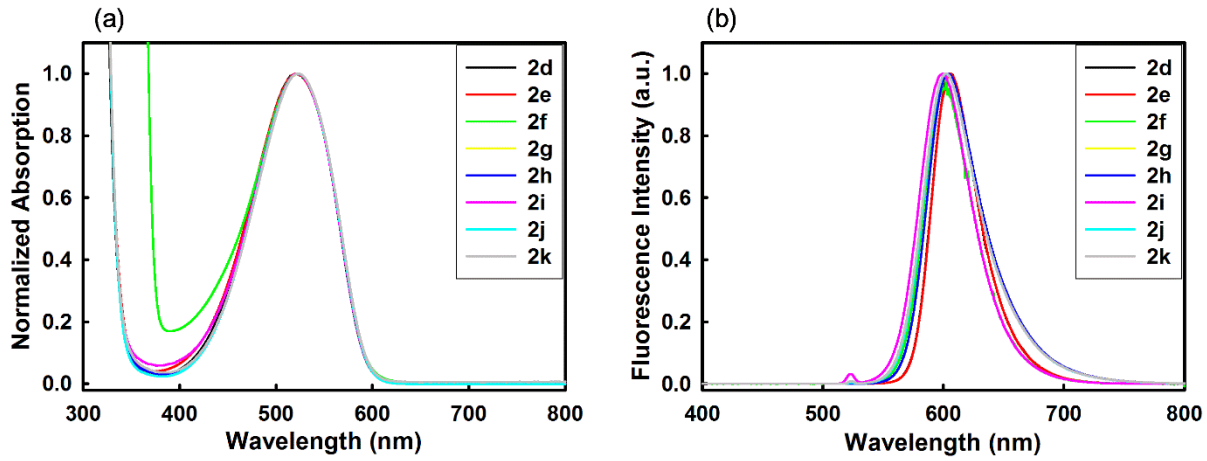

Figure 4. UV-Vis absorption and fluorescence spectra of pyrazine dyes **2d**–**2k** in chloroform.

The absorption and fluorescence spectra of pyrazine dyes **2d**–**2k** in the neat state are shown in Fig. 5(a) and (b), respectively. Dyes **2d**–**2k** in the liquid and solid states exhibited strong absorption at approximately 517 nm. The absorption maximum of the solid state dyes **2j** and **2k** slightly shifted to longer

wavelengths relative to the maximum of the liquid state dyes **2d**–**2i**. In contrast, dyes **2d**–**2k** absorbed at shorter wavelengths than dyes **2a**–**2c** which contain short alkyl chain length substituents. It was assumed that the steric hindrance between the molecules decreased intermolecular π-π interactions in dyes **2d**–**2k**. The fluorescence spectra of dyes **2d**–**2k** showed a sharp fluorescent band at 598–604 nm. In the neat form, dyes **2d**–**2i** showed no considerable difference in their optical properties except for fluorescence efficiency. This is likely due to the similar liquid phase structure and electronic properties in chloroform solution. In contrast, the derivatives containing a long alkyl chains (**2j** and **2k**) showed the same characteristics including fluorescence quantum yield in solution as in the solid state. In this case, the long alkyl chains weakened the intermolecular interactions between the chromophores that affect the electronic states of the solids and formed an electronic state similar to that observed in solution, though it is necessary to analyse the crystal structure for confirmation. Furthermore, the liquid derivatives were fluorescent in their neat form. All neat state pyrazine dyes showed fluorescence quantum yields ranging from 0.04 to 0.59. The liquid dyes reported to date are known to exhibit generally low fluorescence quantum yields in the liquid state.[1,2,5,31–33] In contrast, the results presented herein showed that the fluorescence quantum yields in the liquid state of dyes **2g**–**2i** were more intense than those of other liquid derivatives.

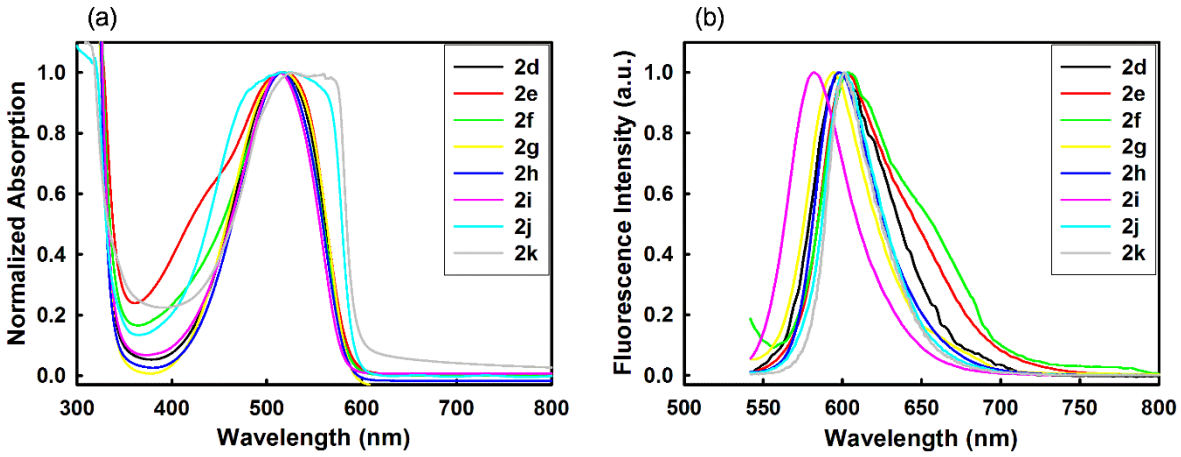

Figure 5. UV-Vis absorption and fluorescence spectra of neat pyrazine dyes **2d**–**2k**.

The absorption properties of dyes **2d**–**2k** were characterised by molecular orbital calculation. The optimised molecular structure was obtained using DFT at the B3LYP/6-31G+(d,p) level of theory, and TD-DFT calculations were subsequently performed using the same basis set. The calculated results are shown in Table 2, which indicate that the geometrically optimised dyes **2d**–**2k** exhibited visible absorption at approximately 506 nm with an oscillator strength of 0.05. This is qualitatively in good agreement with the solution absorption characteristics. The HOMO to LUMO transition was a major component for the visible

absorption band. Both the observed and calculated results showed that the absorption maximum of dyes **2d**–**2k** was not significantly affected by increased length of the alkyl chain.

Table 2. Excitation energies, oscillator strengths, and major components calculated for dyes **2d**–**2k**.

Compound	*E* (eV, nm)	*f*	Major component	λ_{max}[a] (nm)
2d	2.46 (505)	0.05	HOMO→LUMO 98%	521
2e	2.45 (505)	0.05	HOMO→LUMO 98%	521
2f	2.45 (506)	0.05	HOMO→LUMO 98%	521
2g	2.45 (506)	0.05	HOMO→LUMO 98%	523
2h	2.45 (506)	0.05	HOMO→LUMO 98%	523
2i	2.45 (506)	0.05	HOMO→LUMO 98%	523
2j	2.45 (506)	0.05	HOMO→LUMO 98%	523
2k	2.45 (506)	0.05	HOMO→LUMO 98%	523

[a]Observed λ_{max} in chloroform.

3.3. Electrochemical properties

In this study, liquid dye **2i** was used as the emitter in an OLED because it exhibited the highest fluorescence quantum efficiency in the liquid state among the prepared liquid pyrazine dyes. To pursue the application possibilities of liquid dye **2i**, its electrochemical properties were further examined. Figure 6 shows the cyclic voltammetric curves of dye **2i**. The measurement was performed using a standard three-electrode electrochemical cell in an electrolyte solution (0.1 M $TBAPF_6$/DCM) with ferrocene as an external reference. The liquid form of dye **2i**, which was prepared on a glassy carbon electrode from a CH_2Cl_2 solution, displayed a single redox peak at a 0.5–1.0 V scanning range with a scan rate of 100 mV/s. The HOMO energy level estimated from the onset potentials of the observed oxidation peak was -5.47 eV, while the LUMO energy level of dye **2i** measured by the HOMO energy level and the optical band gap energy (E_g) obtained from the onset of the absorption spectra by extrapolation was -3.35 eV. The HOMO and LUMO energy levels were determined using previously reported equations. [34,35]

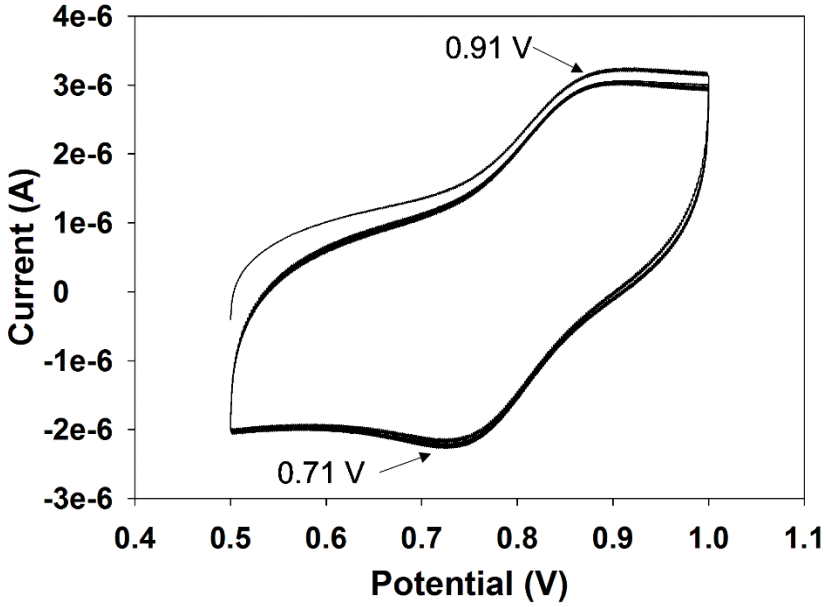

Figure 6. CV curves of dye **2i**.

3.4. Electroluminescent properties of 2i

The electroluminescent properties of liquid dye **2i** were measured using a device composed of ITO / PEDOT : PSS / TmPyPB (35 nm) / **2i** : F8BT / LiF (0.6 nm) /Al (80 nm). The emitting layer was composed of 60 wt% **2i** and 40 wt% F8BT. Dye **2i** was used in a dispersed state in a high efficiency green-yellow emitting luminescent polymer because it was difficult to fix on a substrate. To determine an appropriate ratio of these two components with respect to the PL properties, PL spectra were measured in a F8BT film, **2i**, and **2i**-doped F8BT films. Figure 7 shows the PL characteristics of **2i** and F8BT spin coated films. The excitation wavelength for the spin coat sample was 468 nm and 100 wt% **2i** was 542 nm. As the concentration of **2i** increased in the spin coated films, the PL intensity of F8BT decreased. This indicates that the energy transfer can effectively occur from F8BT to **2i** with increasing concentration of **2i**. The energy transfer likely occurred through the overlap of the emission spectrum of F8BT and absorption spectrum of **2i** (Fig. S1). When the ratio of **2i** in the spin coated film was >60 wt%, the liquid dye content is high, so the film becomes soft and hard to fix on the substrate. Therefore, a ratio of **2i** to F8BT of 60 wt%:40 wt% was selected.

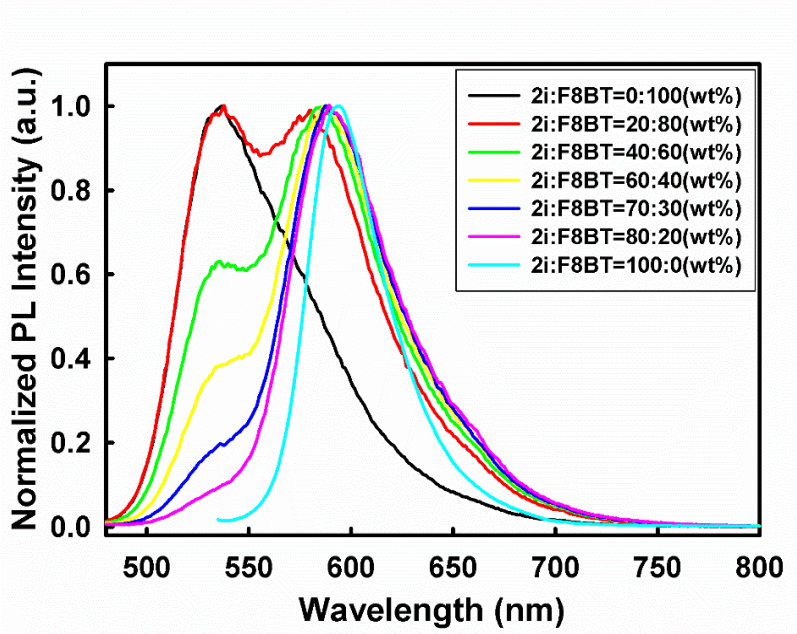

Figure 7. PL spectra of **2i** and F8BT spin coated films prepared at different ratios (λ_{ex}=468 nm for **2i**:F8BT=0:100~80:20 wt%, λ_{ex}=542 nm for **2i**:F8BT=100:0 wt%).

Figure 8 shows the normalised EL spectra at 13 V. The device emits yellow light with a maximum of 593 nm and the EL spectral shape was nearly identical to the previously discussed PL emission spectra of **2i**. This indicated that the EL of **2i** and F8BT spin coated films exhibited the same photophysical properties in terms of excitation and emission as the energy transfer of PL.

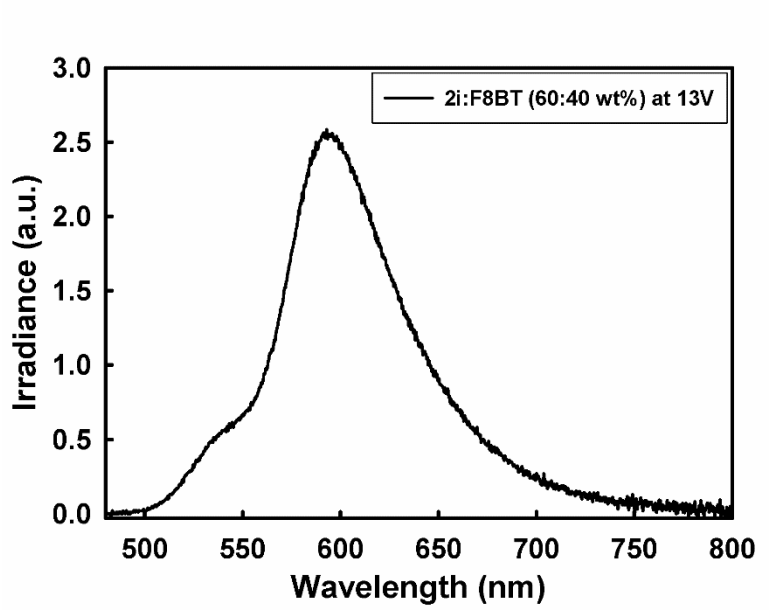

Figure 8. EL spectra of dye **2i**:F8BT (60:40 wt%) at 13 V.

The current density-voltage (*J*-*V*) and luminescence-voltage (*L*-*V*) characteristics of the prepared device are presented in Fig. 9. The current increased constantly with increasing applied voltage and the turn-on voltage of luminance at 1 cd/m^2 was approximately 10 V. The fabricated device showed the highest luminance of 336 cd/m^2 at 14 V. Although the device characteristics are quite primitive compared with those of the well-established OLEDs containing liquid dyes [36–38], the results shown in Figs. 8 and 9 indicate that the liquid fluorescent dye **2i** has good potential as an emission material in OLEDs.

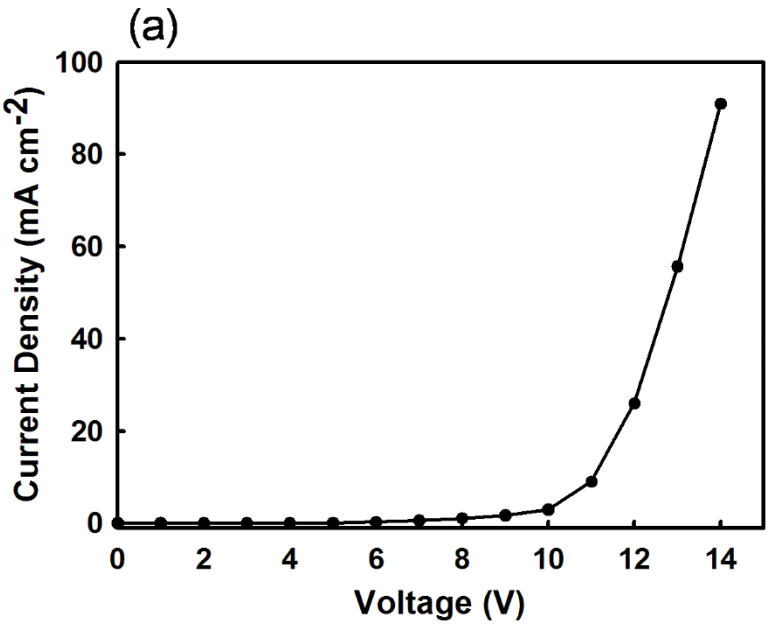

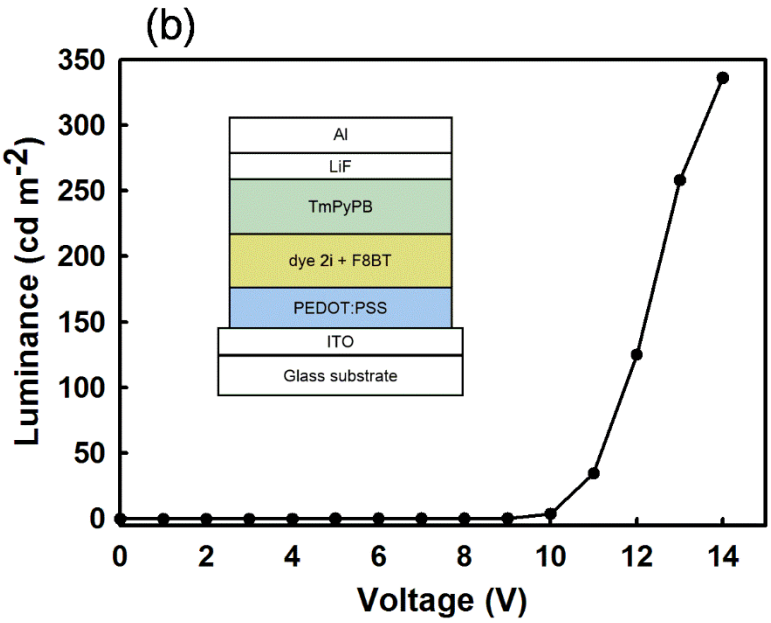

Figure 9. (a) *J*-V and (b) *L*-V characteristics of the prepared OLED (ITO/PEDOT:PSS/**2i**:F8BT (60:40 wt%)/TmPyPB/LiF:Al). Inset: schematic drawing of the OLED cross-section.

4. Conclusion

In summary, liquid pyrazine dyes were synthesised by altering the alkyl substituent chain length on the amino groups in 2,5-bis(dialkylamino)-3,6-dicyanopyrazine. The alkyl group in the dye system drastically affected the melting point of the dyes. The butyl, pentyl, hexyl, heptyl, octyl, and dodecyl derivatives were liquids at room temperature, whereas the methyl, ethyl, propyl, hexadecyl, and octadecyl derivatives were solids under the same conditions. All derivatives exhibited medium to high fluorescence quantum yields ranging from 0.45 to 0.73 in chloroform. In addition, the liquid derivatives were fluorescent in their neat form. The dodecyl derivative exhibited excellent fluorescence emission and appropriate energy levels, which could be utilised as emitting materials for OLED devices. The OLED device fabricated with an emitting layer consisting of liquid dye **2i** and F8BT showed efficient yellow EL emission at 593 nm. The turn-on voltage of the device was 10 V with a maximum brightness of 336 cd/m^2 at 14 V. This is a preliminary result and further optimisation of the device structure and preparation conditions must be performed.

References

[1] Hirata S, Heo HJ, Shibano Y, Hirata O, Yahiro M, Adachi C. Improved device lifetime of organic light emitting diodes with an electrochemically stable π-conjugated liquid host in the liquid emitting layer. Jpn J Appl Phys 2012;51:041604. https://doi.org/10.1143/JJAP.51.041604

[2] Xu D, Adachi C. Organic light-emitting diode with liquid emitting layer. Appl Phys Lett 2009;95:053304. https://doi.org/10.1063/1.3200947

[3] Tsuwaki M, Kasahara T, Edura T, Matsunami S, Oshima J, Shoji S, et al. Fabrication and characterization of large-area flexible microfluidic organic light-emitting diode with liquid organic semiconductor. Sens Actuators, A 2014;216:231–6. https://doi.org/10.1016/j.sna.2014.05.032

[4] Kobayashi N, Kasahara T, Edura T, Oshima J, Ishimatsu R, Tsuwaki M, et al. Microfluidic white organic light-emitting diode based on integrated patterns of greenish-blue and yellow solvent-free liquid emitters. Sci Rep 2015;5:14822. https://doi.org/10.1038/srep14822

[5] Kasahara T, Matsunami S, Edura T, Ishimatsu R, Oshima J, Tsuwaki M, et al. Multi-color microfluidic electrochemiluminescence cells. Sens Actuators, A 2014;214:225–9. https://doi.org/10.1016/j.sna.2014.04.039

[6] Ribierre JC, Aoyama T, Muto T, Imase Y, Wada T. Charge transport properties in liquid carbazole. Org Electron 2008;9:396–400. https://doi.org/10.1016/j.orgel.2008.01.005

[7] Ribierre JC, Aoyama T, Muto T, André P. Hybrid organic–inorganic liquid bistable memory devices. Org Electron 2011;12:1800–5. https://doi.org/10.1016/j.orgel.2011.07.007

[8] Park SY, Kubota Y, Funabiki K, Matsui M. Survey of liquid coumarin dyes and their fluorescence properties. Chem Lett 2009;38:162–3. https://doi.org/10.1246/cl.2009.162

[9] Biradar S, Shigemitsu Y, Kubota Y, Funabiki K, Sato H, Matsui M. Effects of the alkyl group in (dialkylamino) perfluorophenazines on the melting point and fluorescence properties. RSC Adv 2014;4:59387–96. https://doi.org/10.1039/C4RA09342A

[10] Michinobu T, Okoshi K, Murakami Y, Shigehara K, Ariga K, Nakanishi T. Structural requirements for producing solvent-free room temperature liquid fullerenes. Langmuir 2013;29:5337−44. https://doi.org/10.1021/la400969f

[11] Birada S, Kasugai R, Kanoh H, Nagao H, Kubota Y, Funabiki K, et al. Liquid azo dyes. Dyes Pigments 2016;125:249–58. https://doi.org/10.1016/j.dyepig.2015.10.024

[12] Matsui M, Kubota Y, Funabiki K. Liquid 2-pyridinium styryl dyes having oxaalkyl units. J Jpn Soc Colour Mater 2014;87:187–91. https://doi.org/10.4011/shikizai.87.187

[13] Kato T, Mizoshita N, Kishimoto K. Functional liquid-crystalline assemblies: self-organized soft materials. Angew Chem, Int Ed 2006;45:38–68. https://doi.org/10.1002/anie.200501384

[14] Achelle S, Baudequin C, Plé N. Luminescent materials incorporating pyrazine or quinoxaline moieties. Dyes Pigments 2013;98:575–600. https://doi.org/10.1016/j.dyepig.2013.03.030

[15] Matsuoka M. 8 - Multifunctional dye materials from new dicyanopyrazine chromophores, In: Freeman HS, Peters AT, editors. Colorants for non-textile applications, Elsevier Science, 2000, p. 339–381. https://doi.org/10.1016/B978-044482888-0/50039-8

[16] Kim JH, Matsuoka M, Fukunishi K. Selective topochemical photoreaction of crystallized 2,3-bis(2-phenylethenyl)-4,5-dicyanopyrazines. Chem Lett 1999;28:143-4. https://doi.org/10.1246/cl.1999.143

[17] Okada N, Eto R, Horiguchi-Babamoto E, Kobayashi T, Naito H, Shiro M, et al. Optical properties of three differently colored crystal modifications of a 2,3-dicyanopyrazine dye. Bull Chem Soc Jpn 2015;88:716–21. https://doi.org/10.1246/bcsj.20140409

[18] Akune Y, Hirosawa R, Endo N, Hatano S, Hosokai T, Sato H, et al. Tuning of fluorescence efficiency via local modification of the crystal structure by benzyl groups in polymorphs of a pyrazine dye. CrystEngComm 2017;19:1947–52. https://doi.org/10.1039/C7CE00164A

[19] Shirai K, Yanagisawa A, Takahashi H, Fukunishi K, Matsuoka M. Syntheses and fluorescent properties of 2,5-diamino-3,6-dicyanopyrazine dyes. Dyes Pigments 1998;39:49–68. https://doi.org/10.1016/S0143-7208(98)00008-4

[20] Kim JH, Shin SR, Matsuoka M, Fukunishi K. Self-assembling of aminopyrazine fluorescent dyes and their solid state spectra. Dyes Pigments 1998;39:341–57. https://doi.org/10.1016/S0143-7208(98)00017-5

[21] Akune Y, Gontani H, Hirosawa R, Koseki A, Matsumoto S. The effects of molecular flexibility and substituents on conformational polymorphism in a series of 2,5-diamino-3,6-dicyanopyrazine dyes with highly flexible groups. CrystEngComm 2015;17:5789–800. https://doi.org/10.1039/C5CE01004G

[22] Akune Y, Hirosawa R, Koseki A, Matsumoto S. Role of halogen substituents in a series of polymorphic 2,5-diamino-3,6-dicyanopyrazine derivatives with highly flexible groups. Z Kristallogr 2017;232(5):395–405. https://doi.org/10.1515/zkri-2016-2007

[23] Matsumoto S, Uchida Y, Yanagita M. A series of polymorphs with different colors in fluorescent 2,5-diamino-3,6-dicyanopyrazine dyes. Chem Lett 2006;35:654–5. https://doi.org/10.1246/cl.2006.654

[24] Akune Y, Hirosawa R, Takahashi H, Shiro M, Matsumoto S. Role of flexible bulky groups and weak interactions involving halogens in the vapoluminescence of a metal-free dye. RSC Adv 2016;6:74506–9. https://doi.org/10.1039/C6RA15966D

[25] Hirosawa R, Akune Y, Endo N, Hatano S, Hosokai T, Sato H, et al. A variety of solid-state fluorescence properties of pyrazine dyes depending on terminal substituents. Dyes Pigments 2017;146:576–81. https://doi.org/10.1016/j.dyepig.2017.07.055

[26] Frisch MJ, Trucks GW, Schlegel HB, Scuseria GE, Robb MA, Cheeseman JR, et. al. Gaussian 16 (Revision A.03), Gaussian, Inc., Wallingford CT, 2016.

[27] Lee C, Yang W, Parr RG. Development of the colle-salvetti correlation-energy formula into a functional of the electron density. Phys Rev B 1988;37:785–9. https://doi.org/10.1103/PhysRevB.37.785

[28] Zhang Y, Maginn EJ. Molecular dynamics study of the effect of alkyl chain length on melting points of $[C_nMIM][PF_6]$ ionic liquids. Phys Chem Chem Phys 2014;16:13489−99. https://doi.org/10.1039/C4CP01048E

[29] Nowak-Król A, Gryko D, Gryko DT. Meso-substituted liquid porphyrins. Chem - Asian J 2010;5:904−9. https://doi.org/10.1002/asia.200900693

[30] Collings PJ, Hird M. Introduction to liquid crystals: chemistry and physics. CRC Press; 1997.

[31] Matsui M, Noguchi K, Kubota Y, Funabiki K. Fluorescence properties of novel 6-butyl-2,3-dicyano-7-methyl-6*H*-1,4-diazepine styryl dyes containing ethyleneglycol units. Tetrahedron 2010;66:9396−400. https://doi.org/10.1016/j.tet.2010.09.103

[32] Matsui M, Yamamoto T, Kubota Y, Funabiki K. Survey, fluorescence spectra, and solubility of liquid cyanine dyes. New J Chem 2016;40:10187−96. https://doi.org/10.1039/C6NJ02160C

[33] Machida T, Taniguchi R, Oura T, Sada K, Kokado K. Liquefaction-induced emission enhancement of tetraphenylethene derivatives. Chem Commun 2017;53:2378−81. https://doi.org/10.1039/C6CC09939D

[34] Kulkarni AP, Tonzola CJ, Babel A, Jenekhe SA. Electron transport materials for organic light-emitting diodes. Chem Mater 2004;16:4556−73. https://doi.org/10.1021/cm049473l

[35] Lee SJ, Park JS, Yoon KJ, Kim YI, Jin SH, Kang SK, et al. High-efficiency deep-blue light-emitting diodes based on phenylquinoline/carbazole-based compounds. Adv Funct Mater 2008;18:3922−30. https://doi.org/10.1002/adfm.200800697

[36] Kasahara T, Matsunami S, Edura T, Ishimatsu R, Oshima J, Tsuwaki M, et al. Multi-color microfluidic organic light-emitting diodes based on on-demand emitting layers of pyrene-based liquid organic semiconductors with fluorescent guest dopants. Sens Actuators, B 2015;207:481−9. https://doi.org/10.1016/j.snb.2014.09.101

[37] Hirata S, Kubota K, Jung HH, Hirata O, Goushi K, Yahiro M, et al. Improvement of electroluminescence performance of organic light-emitting diodes with a liquid-emitting layer by

introduction of electrolyte and a hole-blocking layer. Adv Mater 2011;23:889−93. https://doi.org/10.1002/adma.201003505

[38] Kubota K, Hirata S, Shibano Y, Hirata O, Yahiro M, Adachi C. Liquid carbazole substituted with a poly(ethylene oxide) group and its application for liquid organic light-emitting diodes. Chem Lett 2012;41:934936. https://doi.org/10.1246/cl.2012.934